International Journal of Research and Technology in Electrical Industry

journal homepage: ijrtei.sbu.ac.ir

Shahid Beheshti University

Design and Comparative Analysis of Multiple MIMO Controllers for a Half-Car Suspension System

Aliakbar Ghasemzadeh[1],Elham Amini Boroujeni[*1]

[1]*Department of Electrical and Computer Engineering, Engineering Faculty, Kharazmi University, Tehran, Iran*

ARTICLE INFO

ABSTRACT

Article history:
Received: 12 August 2024
Revised: 08 October 2024
Accepted: 21 October 2024

Keywords:
Half-car suspension
MIMO control
PID control
H_∞ control
Vibration attenuation

This paper investigates the design of multiple-input multiple-output (MIMO) controllers for a half-car suspension system, aiming to enhance ride quality by minimizing displacement and angular deviations. The nonlinear equations describing the half-car model are derived, incorporating control inputs and road disturbances. The study explores centralized, decentralized, and semi-centralized (sequential) control strategies using proportional-integral (PI), proportional-integral-derivative (PID), and H_∞ robust control techniques. The centralized PI and H_∞ controllers are designed using Markov parameters and sensitivity weighting functions, respectively. In the decentralized approach, control designs involve inverse decoupling, state feedback decoupling, PID tuning against disturbances, and mixed-sensitivity H_∞ optimization. The semi-centralized strategy sequentially closes control loops using a PID architecture. Extensive simulations are conducted with step and road bump disturbance inputs applied to the closed-loop system. Controller performance is evaluated based on displacement suppression, control effort, settling time, and robustness to external shocks. The proposed decentralized H_∞ controller achieves superior vibration attenuation to the picometer level while exhibiting strong disturbance rejection capabilities. The comparative analysis underscores the advantages of the developed control schemes over existing solutions, contributing to enhanced passenger comfort in automotive suspension systems.

1. Introduction

Active suspension systems for vehicle seats have garnered substantial research attention due to their potential to improve ride quality and isolate passengers from vibrations originating in the vehicle body and road disturbances [1]-[26]. Sophisticated control methodologies have enabled active seat suspensions to mitigate vibrations across a wide band of frequencies adaptively. Recent studies have developed robust optimization approaches to deal with uncertainties and disturbances for full vehicle models, such as multi-objective optimization [1], intelligent, active force control schemes [2], event-triggered H_∞ control [3], and event-triggered state feedback [4].

Significant work has also focused on control design and modeling for half-car suspension systems, including modeling and simulation [5], adaptive vehicle stability control [6], comparative analysis of techniques like PID, LQR, fuzzy logic, and ANFIS [7], feedback linearization, and LQR control [8], sliding mode control [9], and

* Corresponding author
E-mail address: e_amini_b@yahoo.com
https://orcid.org/0000-0002-6762-477X
http://dx.doi.org/10.48308/ijrtei.2024.236572.1056

optimal state-feedback control [10]. Other robust solutions for full vehicle systems include a linear matrix inequality (LMI) technique for a semi-active electrorheological damper [11] and a methodology for general suspension parametric uncertainty [12].

Intelligent control strategies have also been explored for full vehicle systems, including fuzzy logic controllers [13, 14] and genetic algorithm optimization of fractional-order PID gains [15]. A key application area has been off-road vehicle seats [16, 17], which experience aggressively uneven terrain and require vibration attenuation over large amplitudes. Investigations have tailored solutions to this setting through model-free control not relying on function approximation [18]. Unique actuator concepts have also been conceived, such as a prototype electromagnetic stiffness element enabling energy recovery [19].

Beyond advanced control techniques, modeling seat mechanical properties for full vehicle systems has received attention to capturing multi-linkage cushion dynamics [20] and seat-passenger coupling [21]. While most research has focused on vertical oscillations, some have addressed multiple degrees of freedom encompassing roll and pitch [22, 23] to better represent the rotation of real automobile seats over uneven ground.

Research has also explored the concept of fault tolerance [24] and time delay reduction [25] to advance the real-world feasibility of full-vehicle active seat suspensions. Moreover, alternative actuators have been tested, including sliding mode controlled electromagnetic suspensions [26], showing promise over conventional hydraulic or pneumatic schemes. The wide array of advanced solutions illustrates the extensive work towards refining active seat suspension performance and deployment capability for both full and half-vehicle models.

The controllers designed for the half-car suspension system to date are both intricate and tend to transmit significant displacements to the vehicle's floor. This paper articulates the equations governing the half-car suspension system, detailing the application of control inputs and disturbances. Subsequently, we present designs for centralized, decentralized, and semi-centralized (sequential) controllers utilizing various approaches, including Proportional-Integral (PI), Proportional-Integral-Derivative (PID), and H_∞ control strategies. The simulation results illustrating the car's floor displacement and angular changes are then provided, along with a comparative analysis against previous studies. The findings indicate a notable improvement in displacement performance relative to earlier methods.

This paper is organized as follows: Section 1 presents the state space and disturbance equations governing a half-car suspension system. In Section 2, we design centralized PI and H_∞ controllers, followed by the development of decentralized PI controllers using both a decoupling method with the inverse system matrix and a state feedback approach. Additionally, we explore the implementation of PID and H_∞ controllers. Finally, a semi-centralized PID controller is introduced. Section 3 provides the simulation results and comparative analysis.

2. System Formulation

The suspension system of vehicles has consistently garnered attention since its inception, as an effective suspension system that significantly enhances passenger comfort. This report focuses on a model representing half of a car's suspension system. When the suspension system is adequately designed, there is no need for spring seats to mitigate passenger vibrations; instead, the seat bases remain stable, effectively preventing any shaking. The half-car suspension system under consideration is derived from [27] and illustrated in Fig. 1. It has been optimized to achieve peak performance without control inputs, relying solely on optimization algorithms to identify optimal parameter values, including the stiffness coefficients of the springs and dampers.

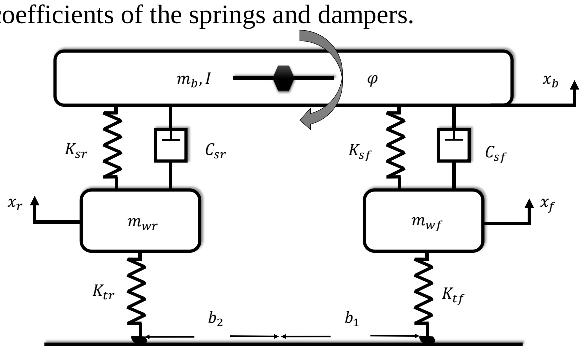

Fig. 1. Half-car suspension system model

Vehicle suspension systems can be modeled as a quarter or half-vehicle model. Fig. 2 represents a modeling of a quarter vehicle suspension system which consists of a wheel and its attachments with mass (M_w) and stiffness (K_t), Sprung mass (M_b), suspension stiffness (K_s), and damping (C_s). The excitation road input is a speed bump whose profile could be modeled as a cosine function as in (1).

$$y_o(t) = \begin{cases} -\frac{H}{2}\left(\cos\left(\frac{2\pi v t}{L}\right) - 1\right), & 0 \le t \le \frac{L}{v} \\ 0, & t > \frac{L}{v} \end{cases} \quad (1)$$

where L and H are the bump’s width and height in order, and v is the velocity of the car passing the bump.

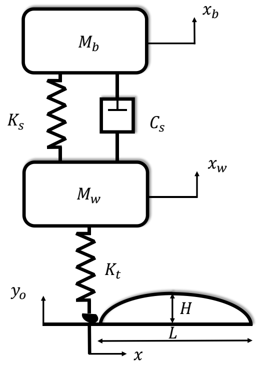

Fig. 2. How to apply perturbation to a car wheel

The optimal performance of this system without control inputs in response to disturbances caused by a vehicle traveling at a speed of 60 km/h over a 0.5 m long and 10 cm high obstacle is illustrated in Fig. 3.

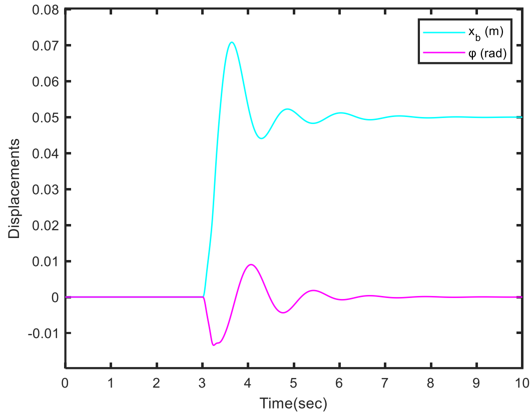

Fig. 3. The best performance of the suspension system with optimization algorithms and without control input.

As illustrated in Fig. 3, the car floor experiences a displacement of approximately 7 cm due to the disturbance, which poses significant risks and discomfort for passengers. The objective of this paper is to mitigate these vibrations to around one nanometer or less.

The dynamic equations of the introduced system are shown in (2).

$$
\begin{aligned}
&m_{\omega f}\ddot{x}_f = -C_{sf}\left(\dot{x}_f + b_1\dot{\varphi} - \dot{x}_b\right) - K_{sf}\left(x_f + b_1\varphi - x_b\right) - K_{tf}x_f + K_{tf}x_{o1} \\
&m_{\omega r}\ddot{x}_r = -C_{sr}(\dot{x}_r - b_2\dot{\varphi} - \dot{x}_b) - K_{sr}(x_r - b_2\varphi - x_b) - K_{tr}x_r + K_{tr}x_{o2} \\
&I\ddot{\varphi} = -C_{sf}b_1\left(b_1\dot{\varphi} + \dot{x}_f - \dot{x}_b\right) - C_{sr}b_2(b_2\dot{\varphi} - \dot{x}_r + \dot{x}_b) - K_{sf}b_1\left(b_1\varphi + x_f - x_b\right) - K_{sr}b_2(b_2\varphi - x_r + x_b) \\
&m_b\ddot{x}_f = -C_{sf}\left(\dot{x}_b - b_1\dot{\varphi} - \dot{x}_f\right) - C_{sr}(\dot{x}_b + b_2\dot{\varphi} - \dot{x}_r) - K_{sf}\left(x_b - b_1\varphi - x_f\right) - K_{sr}(x_b + b_2\varphi - x_r)
\end{aligned}
\tag{2}
$$

Similar to [28], by placing two control inputs in Fig.4 for the system in Fig.1, the state equations of the system change from (2) to (3). In practice, electrohydraulic actuators or permanent magnet linear motors can be used to produce the required forces u_1 and u_2 [11].

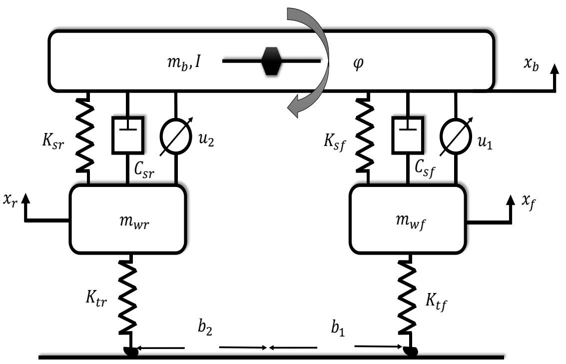

Fig.4. Half-car suspension model with control inputs

Table I. System parameters

Parameter	Symbol	Value
Body mass	m_b	1794 kg
Body inertia	I	3443.5 kg m^2
Front-wheel mass	m_{wf}	87.15 kg
Rear-wheel mass	m_{wr}	140.04 kg
Damping coefficient of front shock absorber	C_{sf}	1190 N s/m
Damping coefficient of rear shock absorber	C_{sr}	1000 N s/m
Front spring coefficient	K_{sf}	66 824.2 N/m
Rear spring coefficient	K_{sr}	18 615 N/m
Spring coefficient of the front tire	K_{tf}	200 000 N/m
Spring coefficient of the rear tire	K_{tr}	200 000 N/m
Front half-length	b_1	1.271 m
Rear half-length	b_2	1.713 m

$$
\dot{x} = Ax + Bu + Ed
$$
$$
y = Cx + Du
$$

$$
A = \begin{bmatrix}
0 & 1 & 0 & 0 & 0 & 0 & 0 & 0 \\
\dfrac{-K_{sf} - K_{tf}}{m_{wf}} & -\dfrac{C_{sf}}{m_{wf}} & 0 & 0 & \dfrac{-K_{sf}b_1}{m_{wf}} & \dfrac{-C_{sf}b_1}{m_{wf}} & \dfrac{K_{sf}}{m_{wf}} & \dfrac{C_{sf}}{m_{wf}} \\
0 & 0 & 0 & 1 & 0 & 0 & 0 & 0 \\
0 & 0 & \dfrac{-K_{sr} - k_{tr}}{m_{wr}} & -\dfrac{C_{sr}}{m_{wr}} & \dfrac{K_{sr}b_2}{m_{wr}} & \dfrac{C_{sr}b_2}{m_{wr}} & \dfrac{K_{sr}}{m_{wr}} & \dfrac{C_{sr}}{m_{wr}} \\
0 & 0 & 0 & 0 & 0 & 1 & 0 & 0 \\
-\dfrac{K_{sf}b_1}{I} & -\dfrac{C_{sf}b_1}{I} & \dfrac{K_{sr}b_2}{I} & \dfrac{C_{sr}b_2}{I} & \dfrac{-K_{sf}b_1^2 - K_{sr}b_2^2}{I} & \dfrac{-C_{sf}b_1^2 - C_{sr}b_2^2}{I} & \dfrac{K_{sf}b_1 - K_{sr}b_2}{I} & \dfrac{C_{sf}b_1 - C_{sr}b_2}{I} \\
0 & 0 & 0 & 0 & 0 & 0 & 0 & 1 \\
\dfrac{K_{sf}}{m_b} & \dfrac{C_{sf}}{m_b} & \dfrac{K_{sr}}{m_b} & \dfrac{C_{sr}}{m_b} & \dfrac{K_{sf}b_1 - K_{sr}b_2}{m_b} & \dfrac{C_{sf}b_1 - C_{sr}b_2}{m_b} & \dfrac{-K_{sf} - K_{sr}}{m_b} & \dfrac{-C_{sf} - C_{sr}}{m_b}
\end{bmatrix}
\tag{3}
$$

$$B=\begin{bmatrix} 0 & 0 \\ -\frac{1}{m_{wf}} & 0 \\ 0 & 0 \\ 0 & -\frac{1}{m_{wf}} \\ 0 & 0 \\ -\frac{b_1}{I} & \frac{b_2}{I} \\ 0 & 0 \\ \frac{1}{m_b} & \frac{1}{m_b} \end{bmatrix},\quad E=\begin{bmatrix} 0 & 0 \\ \frac{K_{tf}}{m_{wf}} & 0 \\ 0 & 0 \\ 0 & \frac{k_{tr}}{m_{wr}} \\ 0 & 0 \\ 0 & 0 \\ 0 & 0 \\ 0 & 0 \end{bmatrix},\quad C=\begin{bmatrix} 0 & 0 & 0 & 0 & 0 & 0 & 1 & 0 \\ 0 & 0 & 0 & 0 & 1 & 0 & 0 & 0 \end{bmatrix},\quad D=\begin{bmatrix} 0 & 0 \\ 0 & 0 \end{bmatrix}$$

The values of nominal and optimized system parameters can be seen in Table I and Table II.
As a result, the state space of the system is represented in the form specified in equation (4).

Table II. Optimized system parameters

	Lower bound	Upper bound	Optimum solution
C_{sf}	1000	2500	2497.9
K_{sf}	10 000	70 000	28 949.4
C_{sr}	1000	2500	2494.5
K_{sr}	10 000	70 000	11 115.7

$$A=10^3\begin{bmatrix} 0 & 0.0010 & 0 & 0 & 0 & 0 & 0 & 0 \\ -2.6271 & -0.0287 & 0 & 0 & -0.4222 & -0.0364 & 0.3322 & 0.0287 \\ 0 & 0 & 0 & 0.0010 & 0 & 0 & 0 & 0 \\ 0 & 0 & -1.5075 & -0.0286 & 0.1360 & 0.0305 & 0.0794 & 0.0178 \\ 0 & 0 & 0 & 0 & 0 & 0.0010 & 0 & 0 \\ -0.0107 & -0.0009 & 0.0055 & 0.0012 & -0.0231 & -0.0033 & 0.0052 & -0.0003 \\ 0 & 0 & 0 & 0 & 0 & 0 & 0 & 0.0010 \\ 0.0161 & 0.0014 & 0.0062 & 0.0014 & 0.0099 & -0.0006 & -0.0223 & -0.0028 \end{bmatrix}$$

$$B=\begin{bmatrix} 0 & 0 \\ -0.0115 & 0 \\ 0 & 0 \\ 0 & -0.0071 \\ 0 & 0 \\ -0.0004 & 0.0005 \\ 0 & 0 \\ 0.0006 & 0.0006 \end{bmatrix},\quad E=10^3\begin{bmatrix} 0 & 0 \\ 2.2949 & 0 \\ 0 & 0 \\ 0 & 1.4282 \\ 0 & 0 \\ 0 & 0 \\ 0 & 0 \\ 0 & 0 \end{bmatrix} \tag{4}$$

$$C=\begin{bmatrix} 0 & 0 & 0 & 0 & 0 & 0 & 1 & 0 \\ 0 & 0 & 0 & 0 & 1 & 0 & 0 & 0 \end{bmatrix},\quad D=\begin{bmatrix} 0 & 0 \\ 0 & 0 \end{bmatrix}$$

By transforming the system representation from state space to transfer function form, the system is represented as shown in equation (5):

$$G=\begin{bmatrix} G_{11} & G_{12} \\ G_{21} & G_{22} \end{bmatrix}$$

$$G=$$

$$G_{11}=\frac{0.00055741(s^2+3.451s+16.27)\,(s^2+28.88s+1448)\,(s^2+2295)}{(s^2+\ 3.239s+15.36)\,(s^2+2.018s+26.52)\,(s^2+28.87s+1451)\,(s^2+29.24s+2572)}$$

$$G_{12}=\frac{0.00055741(s^2+2.134s+28.5)\,(s^2+10.81s+1428)\,(s^2+29.28s+2568)}{(s^2+\ 3.239s+15.36)\,(s^2+2.018s+26.52)\,(s^2+28.87s+1451)\,(s^2+29.24s+2572)} \tag{5}$$

$$G_{21}=\frac{-0.00036915\,(s^2+3.028s+14.27)\,(s^2+28.86s+1456)\,(s^2+2295)}{(s^2+\ 3.239s+15.36)\,(s^2+2.018s+26.52)\,(s^2+28.87s+1451)\,(s^2+29.24s+2572)}$$

$$G_{22}=\frac{0.00049752(s^2+1.877s+25.05)\,(s^2+10.81s+1428)\,(s^2+29.21s+2575)}{(s^2+\ 3.239s+15.36)\,(s^2+2.018s+26.52)\,(s^2+28.87s+1451)\,(s^2+29.24s+2572)}$$

$G_d =$

$$G_{11} = \frac{3195.3\ (s+11.59)\ (s^2+3.451s+16.27)\ (s^2+28.88s+1448)}{(s^2+\ 3.239s+15.36)\ (s^2+2.018s+26.52)\ (s^2+28.87s+1451)\ (s^2+29.24s+2572)}$$

$$G_{12} = \frac{1985.8\ (s+4.456)\ (s^2+2.134s+28.5)\ (s^2+29.28s+2568)}{(s^2+\ 3.239s+15.36)\ (s^2+2.018s+26.52)\ (s^2+28.87s+1451)\ (s^2+29.24s+2572)}$$

$$G_{21} = \frac{-2116.1\ (s+11.59)\ (s^2+3.028s+14.27)\ (s^2+28.86s+1456)}{(s^2+\ 3.239s+15.36)\ (s^2+2.018s+26.52)\ (s^2+28.87s+1451)\ (s^2+29.24s+2572)}$$

$$G_{22} = \frac{1772.5\ (s+4.456)\ (s^2+1.877s+25.05)\ (s^2+29.21s+2575)}{(s^2+\ 3.239s+15.36)\ (s^2+2.018s+26.52)\ (s^2+28.87s+1451)\ (s^2+29.24s+2572)}$$

Investigating the open-loop behavior of the system and analyzing the poles and zeros leads that we are dealing with a stable and non-minimum phase system. In addition, an examination of the controllability and observability matrices indicates that all states are controllable and observable.

3. Controller Design

In this section, robust PI, and H_∞ controllers are designed in various ways such as centralized, semi-centralized, and decentralized for the system (5).

3.1. Centralized Controller

3.1.1 Centralized PI Controller

First, a centralized PI controller for the system (5) is designed using Markov parameters. For this purpose, by calculating the CB and G(0) matrices of the system, Equations (6) and (7) are obtained:

$$CB = \begin{bmatrix} 2\times10^{-5} & \dfrac{3\times10^{-4}}{8} \\ -2\times10^{-5} & 0.35\times10^{-4} \end{bmatrix} \tag{6}$$

$$\rightarrow (CB)^{-1} = 10^4 \begin{bmatrix} 2.4138 & -2.5862 \\ 1.3793 & 1.3793 \end{bmatrix}$$

$$G(0) = 10^{-4} \begin{bmatrix} 0.1982 & 0.3832 \\ -0.1158 & 0.3015 \end{bmatrix}$$

$$\rightarrow (G(0))^{-1} = 10^4 \begin{bmatrix} 2.8946 & -3.6796 \\ 1.1118 & 1.9036 \end{bmatrix} \tag{7}$$

By considering design tips and choosing proper coefficient ε, K_{P1} *and* K_{P2} examining the stability of PI controller coefficients, they will be in the form of (8) and (9).

$$K_P = (CB)^{-1} \times \begin{bmatrix} K_{P1} & 0 \\ 0 & K_{P2} \end{bmatrix}$$
$$= 10^4 \begin{bmatrix} 2.4138 & -2.5862 \\ 1.3793 & 1.3793 \end{bmatrix} \times \begin{bmatrix} 6 & 0 \\ 0 & 7 \end{bmatrix} \tag{8}$$
$$= 10^5 \begin{bmatrix} 1.4483 & -1.8103 \\ 0.8276 & 0.9655 \end{bmatrix}$$

$$K_i = \varepsilon \times \left(\mathrm{G}(0)\right)^{-1}$$
$$= 0.2 \times 10^4 \begin{bmatrix} 2.8946 & -3.6796 \\ 1.1118 & 1.9036 \end{bmatrix} \tag{9}$$
$$= 10^3 \begin{bmatrix} 5.7891 & -7.3593 \\ 2.2236 & 3.8072 \end{bmatrix}$$

3.1.2. Centralized H_∞ Controller

In this section, a centralized robust H_∞ controller will be designed with a sensitivity weighting function (10) and input weight function (11). The controller's transfer function matrix is determined as (12). The block diagram of this method is presented in Fig.5.

$$W_s = 0.1 \begin{bmatrix} \dfrac{0.066667\ (s+11.45)^\wedge 3}{(s+0.2154)^\wedge 3} & 0 \\ 0 & \dfrac{0.066667\ (s+11.45)^\wedge 3}{(s+0.2154)^\wedge 3} \end{bmatrix} \tag{10}$$

$$W_u = \begin{bmatrix} 10^{-11} & 0 \\ 0 & 10^{-11} \end{bmatrix} \tag{11}$$

$$K = \begin{bmatrix} \dfrac{4.432e11\, s^{13} +\ 2.169e15\, s^{12} + \cdots}{s^{14} + 9959\, s^{13} + 4.956e07\, s^{12} + \cdots} & \dfrac{-3.935e11\, s^{13} -\ 2.168e15\, s^{12} + \cdots}{s^{14} + 9959\, s^{13} + 4.956e07\, s^{12} + \cdots} \\ \dfrac{3.863e11\, s^\wedge 13\ +\ 1.751e15\, s^\wedge 12}{s^{14} + 9959\, s^{13} + 4.956e07\, s^{12} + \cdots} & \dfrac{4.447e11\, s^{13} +\ 2.293e15\, s^{12} + \cdots}{s^{14} + 9959\, s^{13} + 4.956e07\, s^{12} + \cdots} \end{bmatrix} \tag{12}$$

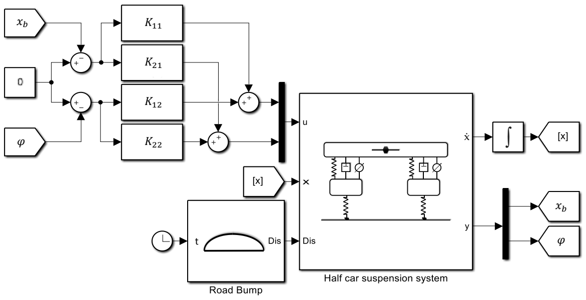

Fig.5. Block diagram of centralized method

3.2. Decentralized Controller

3.2.1 PI first method

In this method, it has been tried to decouple the system. However, due to the absence of matrix D, the system is strictly proper, making its inverse is impossible. To address this issue, a fast pole is introduced in the inverse of the system. Consequently, the product of G and G_{inv} results in an almost decoupled system.

To eliminate the steady-state error of the decoupled system, a simple integrator is employed along with an appropriate gain. This configuration ensures that the permanent error is effectively reduced to zero, as illustrated in the block diagram in Fig. 6. This approach simplifies the control design while maintaining robust performance in managing disturbances.

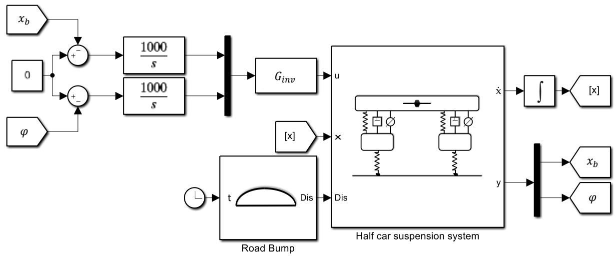

Fig.6. Block diagram of the first decentralized PI method

3.2.2 PI second method

In this method, the static state feedback matrix is utilized to transform the system's transfer function into a decoupling form featuring four poles at the origin. This configuration allows for the implementation of a controller, as illustrated in the block diagram in Fig. 7, to achieve zero steady-state error and rapid response speed.

In this method, B^* and $\bar{B}$ matrices are calculated according to Eq. (13) which leads the formulation of the controller as follows:

$$u = \left(B^*\right)^{-1}\left[-\bar{B}x(t) + \upsilon(t)\right]$$

$$D_d = \begin{bmatrix} s^2 & 0 \\ 0 & s^2 \end{bmatrix},$$

$$B^* = D_d G = 10^{-3}\begin{bmatrix} 0.55741 & 0.55741 \\ -0.36915 & 0.49752 \end{bmatrix}$$

or

$$B^* = \begin{bmatrix} C_1AB \\ C_2AB \end{bmatrix} = 10^{-3}\begin{bmatrix} 0.55741 & 0.55741 \\ -0.36915 & 0.49752 \end{bmatrix}, \tag{13}$$

$$\bar{B} = \begin{bmatrix} C_1A^2B \\ C_2A^2B \end{bmatrix} = \begin{bmatrix} 16.1368 & 1.3924 & 6.196 & 1.3905 & 9.896 & -0.6122 & -22.3328 & -2.7828 \\ -10.6867 & -0.9221 & 5.5303 & 1.2411 & -23.0562 & -3.2979 & 5.1563 & -0.319 \end{bmatrix}$$

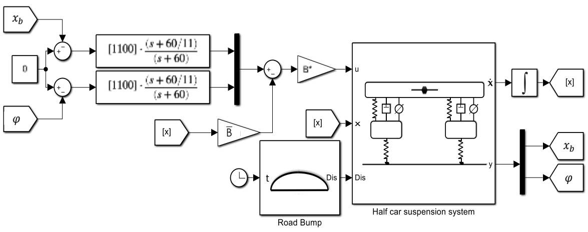

Fig.7. Block diagram of the second decentralized PI method

3.2.3. Decentralized PID Controller

In the decentralized PID controller design, a controller is designed for the G_{11} transfer function and a controller for the G_{22} transfer function separately using the tuning block PID. This method does not consider G12 for the first output and G21 for the second output. Simultaneously, the G_d transfer function is also the perturbation transfer function for the whole system. PID controllers' coefficients $\left(P + \frac{I}{s} + \frac{DN}{1+\frac{N}{s}}\right)$ of the first and second loops are the same and described in (14). The block diagram of this method is depicted in Fig.8.

$$P = 16478731.7,\ I = 4596137.5,$$
$$D = 13127303.4,\ N = 5463.7 \tag{14}$$

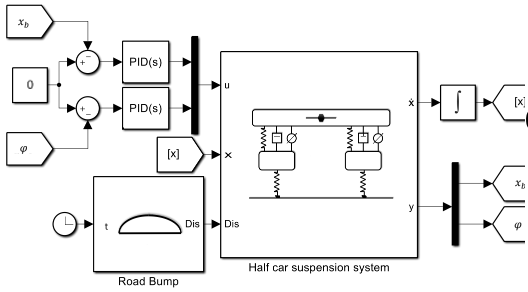

Fig.8. Block diagram of decentralized PID method

3.2.4. Decentralized H_∞ Controller

In this section, the H_∞ method is employed to design a robust controller, wherein the disturbance transfer function and the two transfer functions G_{12}, and G_{21} are not included in the block diagram for the H_∞ code. Instead, similar to section 3.2.1, the inverse transfer function G_{inv} is utilized for decoupling the system. Subsequently, two Single-Input Single-Output (SISO) controllers are designed for the G_{11}, and G_{22} transfer functions using input weight functions as defined in equation (16). H_∞ controllers of first and second loops are described in (17). Additionally, the block diagram of this method is depicted in Fig.9.

$$W_s = \frac{-0.1634s^{12} + 4617s^{11} + \cdots}{s^{14} + 188.6s^{13} + 3.397e04s^{12}} \tag{15}$$

$$W_u = 10^{-11} \tag{16}$$

$$K = \begin{bmatrix} \dfrac{5.21e08s^{15} + 9.137e12s^{14} + \cdots}{s^{16} + 3.778e05s^{15} + 1.956e10s^{14} + \cdots} & 0 \\ 0 & \dfrac{5.21e08s^{15} + 9.137e12s^{14} + \cdots}{s^{16} + 3.778e05s^{15} + 1.956e10s^{14} + \cdots} \end{bmatrix} \tag{17}$$

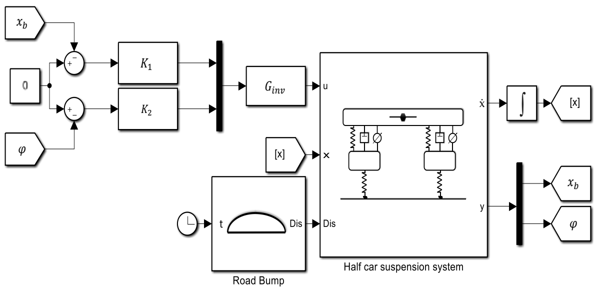

Fig.9. Block diagram of decentralized H_∞ method

3.3. Semi-Centralized (Sequential) Controller

In this method, the first control loop is closed by considering subsystem G_{12} in the presence of the interference effect of subsystem G_{11}, and then the second loop is closed by considering the first one. The pairing of inputs and outputs is similar to the decentralized method. That is, the second input should be used to control the first output, and the first input should be used to control the second output. In the next step, the second control loop must be closed, considering that the first loop is already closed. By considering the mentioned points and examining the stability of the system, the controllers are obtained as (18) and (19).

P = -9145780.33, I = -28291844.5, D = -656903, N = 60598.27 (18)

P = 64285555.48, I = 437610052.9, D = 2098265.71, N = 133350.2 (19)

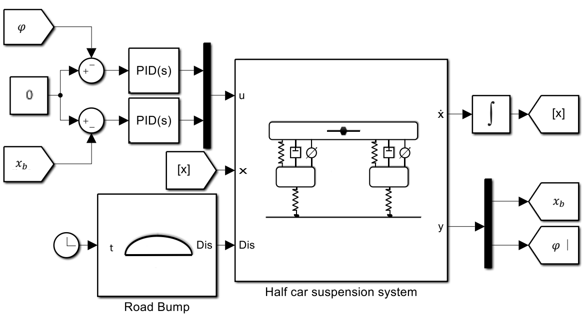

Fig.10. Block diagram of Sequential control

4. Simulation Results

As explained in Section 2, the understudying half-Car Suspension System is a stable and non-minimum phase system. The best performance of this system without control input against the disturbance caused by the passing of a car at a speed of 60 km/h through a 0.5 m long and 10 cm high obstacle is shown in Fig.3.

In this section, the closed-loop system is analyzed using the PI, PID, and H_∞ MIMO controllers designed in the previous section. It should be noted that in all simulations, the control efforts (u) and its effect on the first (x_b) and second (φ) outputs.

Fig.11 shows the closed-loop behavior of the system with the designed PI centralized controller. As can be seen, the interference effect of the movement over the bump on the outputs at the second 3s has been well rejected. However, it still disrupts the car passengers because the displacement is about millimeters. Also, in less than 20 seconds, the controller can demonstrate its robustness against disturbance.

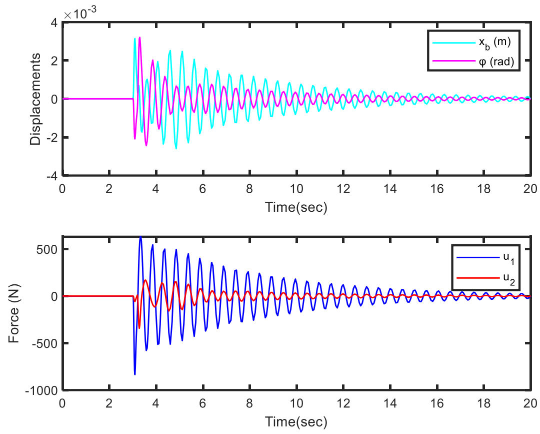

Fig.11. Simulation results of PI Centralized control

Fig.12 shows the output response with centralized H_∞ control, due to the nature of this type of controller, it has been able to have better performance with more control effort.

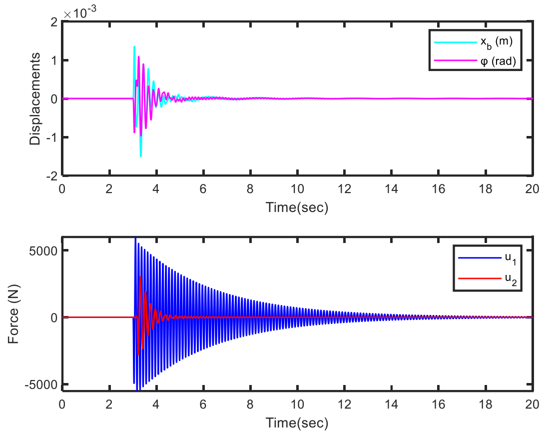

Fig.12. Simulation results of centralized H_∞ control

The response to the external disturbance by the PI controllers, with the decoupling method using system inversion and with the state feedback method, is depicted in Fig.13 and 14, respectively. As can be seen, the first method has reduced the displacement by about µm due to using the decoupler transfer function in addition to the PI controller. On the other hand, the second method has given the best answer among the other PI controllers due to the use of two closed loops. Thus, the movement will not be felt practically because it is about nanometres.

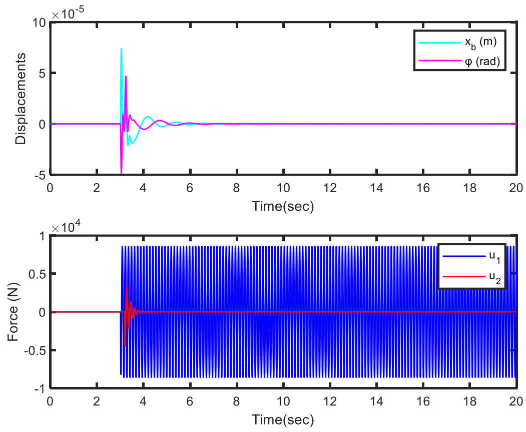

Fig.13. Simulation results of first decentralized PI control

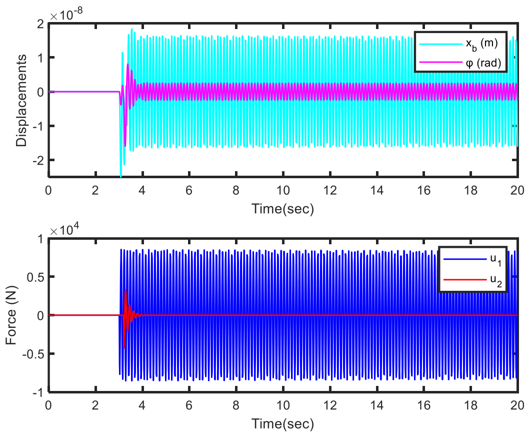

Fig.14. Simulation results of second decentralized PI control

The decentralized PID controller shown in Fig.15 takes longer to reduce the displacement within the nm range due to the lack of an additional loop or decoupling matrix.

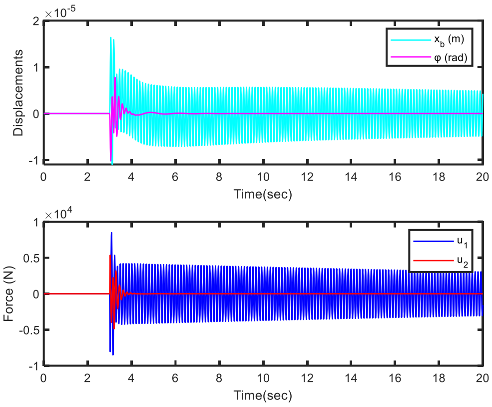

Fig.15. Simulation results of decentralized PID control

Figure 16 illustrates the response of the decentralized H_∞ controller, which outperformed the other controllers in this study. As previously mentioned, the decentralized PI controller, utilizing the inverse method for decoupling, achieved a response of approximately µm with a simple 1/s and a gain. Consequently, due to the enhanced capabilities of the H_∞ method, superior performance was anticipated from this controller.

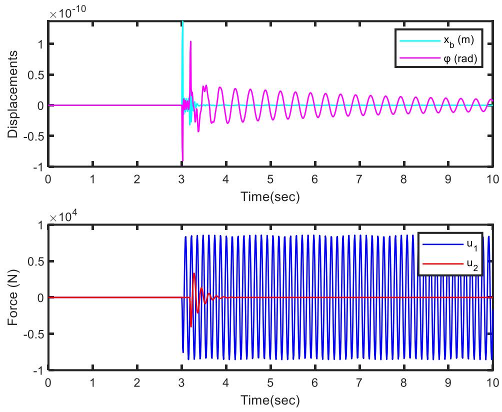

Fig.16. Simulation results of decentralized H_∞Controller

The semi-centralized PID controller is depicted in Fig. 17. By employing the sequential loop closing method, this controller exhibits marginally better performance than the decentralized PID controller, particularly in terms of displacement reduction, although it requires slightly more control effort.

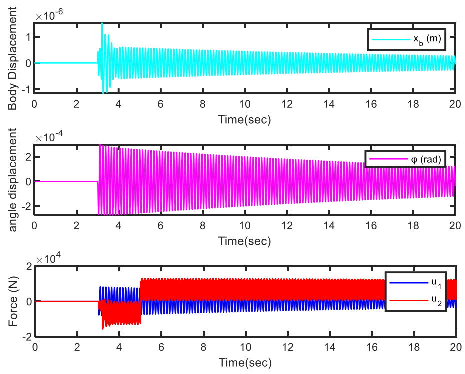

Fig.17. Simulation results of sequential PI Controller

4.1 Comparison

In this part, the designed controllers are compared in terms of controller order, Required Power, and the displacement's overshoot in the half-car suspension system. The brief results are shown in Table III.

Due to its simplicity, the centralized PI controller has the least order and control effort, and as a result, it has more displacement overshoot compared to others. Both decentralized and sequential PID controllers have low order. Moreover, both have reduced displacement overshoot in the order of µm. However, the sequential controller has reduced the displacement overshoot by about 15 micrometers by using power twice the decentralized control effort. While the first decentralized PI control has an acceptable controller order and control effort, it ranks third in terms of displacement overshoot reduction. The best performance among the controllers belongs to the second decentralized PI control, which has a little less control effort than the first decentralized PI method and reduces the displacement overshoot by about nanometers so that the passenger practically does not feel anything about the slips. Nevertheless, it should be noted that this method is a bit difficult to implement in hardware due to feedback from the system's states.

The order of the decentralized H_∞ controller is twice that of the centralized one, and the control effort is a little more. On the other hand, they are not comparable in terms of displacement overshoot because decentralized is around Pico meters, which suggests that no vibration or movement is noticeable for passengers, while centralized is around millimeters.

Table III. Comparison of the designed controllers

Controller	Displacement's overshoot	Required Power	Order of controller
Centralized PI	3 mm	0.8kN	2
Centralized H_∞	1.5 mm	6kN	14
Decentralized PI-1st	70 µm	8kN	11
Decentralized PI- 2nd	25 nm	7.5kN	4
Decentralized PID	17 µm	8kN	2
Decentralized H_∞	190 pm	8kN	26
Sequential PID	1.5 µm	15kN	2

As shown in Table III, the designed controllers in this paper have better performance than ref [6-8] because of their less displacement overshoot.

Regarding Table III, the best controller in this paper is the decentralized H_∞ method with acceptable control effort compared with previous research.

It is while according to Table 1, the mass, inertia, and stiffness of the springs of our system are much higher than the previous research. Thus, it requires more force to control.

Unscented Kalman Filter-based Super Twisting Control (UKF-STC) for a half-car suspension system is presented in [9], while an additional damper is considered. The comparison between this method and our proposed decentralized H_∞ control, in Table IV, shows that our best controller's Root Mean Square Error (RMSE) is much less than [9] as one of the latest research on this subject.

Table IV. Comparison between the proposed decentralized H_∞ and [9]

RMSE ($\times 10^{-11}$)	UKF-STC[9]	Decentralized H_∞
x_b	28.701	8.4467
φ	77.269	2.498

5. Conclusion

This paper has presented a comprehensive investigation into the design of MIMO controllers for the half-car suspension system to minimize displacement and oscillations. The nonlinear dynamical model was formulated, explicitly incorporating control forces and disturbance inputs from road surface irregularities. Centralized, decentralized, and semi-centralized control architectures were systematically developed using robust PI, PID, and H_∞ techniques. The centralized controllers demonstrated effective disturbance rejection capabilities but suffered higher displacement than their decentralized counterparts. Among the decentralized schemes, the H_∞ controller designed via inverse decoupling and mixed-sensitivity optimization, achieves unparalleled vibration suppression performance and curtailing displacements to the Pico meter range amid external shocks. This outstanding attenuation stemmed from the controller's robust characteristics and appropriate selection of frequency-dependent weighting functions tailored to the disturbance dynamics.

The semi-centralized PID controller, leveraging sequential loop closures, offered a practical balance between displacement mitigation and control effort expenditure. A comparative evaluation against previous works substantiated the superiority of the proposed control methodologies, particularly the decentralized H_∞ strategy in improving passenger comfort under realistic driving scenarios. Despite the formidable computational complexity of certain designs, the meticulous treatment of system nonlinearities, input-output interactions, and exogenous disturbances contributed to their exceptional disturbance-nulling capabilities.

While the current study restricted its focus to the half-car model, future research endeavors could extend these advanced control formulations to comprehensive full-vehicle dynamics. Incorporating additional degrees of freedom and practical implementation constraints would further enrich the real-world applicability of the developed schemes.

6. References

[1] G. G. Fossati, L. F. F. Miguel, and W. J. P. Casas, "Multi-objective optimization of the suspension system parameters of a full vehicle model," *Optimization and Engineering*, vol. 20, no. 1, pp. 151-177, 2019.

[2] M. Gohari and M. Tahmasebi, "Active off-road seat suspension system using intelligent active force control," *Journal of Low-Frequency Noise, Vibration and Active Control*, vol. 34, no. 4, pp. 475-489, 2015.

[3] W. Li, J. Wei, H. Du, D. Ning, W. Li, and X. Zhu, "Event-triggered H ∞ control for active seat suspension systems with state delay," *Transactions of the Institute of Measurement and Control*, vol. 43, no. 15, pp. 3428-3437, 2021.

[4] W. Li, H. Du, Z. Feng, D. Ning, and W. Li, "Dynamic output‐feedback event‐triggered H∞ control for singular active seat suspension systems with a human body model," *IET Control Theory & Applications,* vol. 15, no. 4, pp. 594-603, 2021.

[5] A. M. H. Al-Ghanim and A. A. Nassar, "Modeling, simulation, and control of half car suspension system using Matlab/Simulink," *International journal of science and research,* 2018.

[6] Q. Zeng, Y.-J. Liu, and L. Liu, "Adaptive vehicle stability control of half-car active suspension systems with partial performance constraints," *IEEE Transactions on Systems, Man, and Cybernetics: Systems,* vol. 51, no. 3, pp. 1704-1714, 2019.

[7] P. Gandhi, S. Adarsh, and K. Ramachandran, "Performance analysis of half car suspension model with 4 DOF using PID, LQR, FUZZY and ANFIS controllers," *Procedia Computer Science,* vol. 115, pp. 2-13, 2017.

[8] M. A. Khan, M. Abid, N. Ahmed, A. Wadood, and H. Park, "Nonlinear control design of a half-car model using feedback linearization and an LQR controller," *Applied Sciences,* vol. 10, no. 9, p. 3075, 2020.

[9] D. G. Nguyen, K. Ji, T. W. Nguyen, and K. Han, "State-Feedback-Critical Super Twisting Sliding Mode Control for a Half-Car Suspension System," *IEEE Access,* vol. 10, pp. 103200-103211, 2022.

[10] N. Uddin, A. Manurung, and R. N. A. Wijaya, "Optimal state feedback control design of half-car active suspension system," *IAENG International Journal of Applied Mathematics,* vol. 51, no. 3, pp. 1-9, 2021.

[11] A. Bagheri and A. Asghari Ganji, "Robust Control of Electro Rheological Suspension System Based on LMI Approach," *Journal of Modeling in Engineering,* vol. 18, no. 62, pp. 153-163, 2020.

[12] R. Bai and H.-B. Wang, "Robust optimal control for the vehicle suspension system with uncertainties," *IEEE Transactions on Cybernetics,* 2021.

[13] X. Ding, R. Li, Y. Cheng, Q. Liu, and J. Liu, "Design of and Research into a Multiple-Fuzzy PID Suspension Control System Based on Road Recognition," *Processes,* vol. 9, no. 12, p. 2190, 2021.

[14] D. X. Phu, V. Mien, and S.-B. Choi, "A new switching adaptive fuzzy controller with an application to vibration control of a vehicle seat suspension subjected to disturbances," *Applied Sciences,* vol. 11, no. 5, p. 2244, 2021.

[15] S. Gad, H. Metered, A. Bassuiny, and A. Abdel Ghany, "Multi-objective genetic algorithm fractional-order PID controller for semi-active magnetorheologically damped seat suspension," *Journal of Vibration and Control,* vol. 23, no. 8, pp. 1248-1266, 2017.

[16] A. Heidarian and X. Wang, "Review on seat suspension system technology development," *Applied Sciences,* vol. 9, no. 14, p. 2834, 2019.

[17] H. Taghavifar and S. Rakheja, "Multi-objective optimal robust seat suspension control of off-road vehicles in the presence of disturbance and parametric uncertainty using metaheuristics," *IEEE Transactions on Intelligent Vehicles,* vol. 5, no. 3, pp. 372-384, 2019.

[18] J. Na, Y. Huang, Q. Pei, X. Wu, G. Gao, and G. Li, "Active suspension control of full-car systems without function approximation," *IEEE/ASME Transactions on Mechatronics,* vol. 25, no. 2, pp. 779-791, 2019.

[19] D. Ning *et al.*, "An electromagnetic variable stiffness device for semiactive seat suspension vibration control," *IEEE Transactions on Industrial Electronics,* vol. 67, no. 8, pp. 6773-6784, 2019.

[20] L. Zhao, Y. Yu, C. Zhou, and F. Yang, "Modelling and validation of a seat suspension with rubber spring for off-road vehicles," *Journal of Vibration and Control,* vol. 24, no. 18, pp. 4110-4121, 2018.

[21] L. Zhao, C. Zhou, Y. Yu, and F. Yang, "Hybrid modelling of driver seat-cushion coupled system for metropolitan bus," *Journal of Low Frequency Noise, Vibration and Active Control,* vol. 36, no. 3, pp. 214-226, 2017.

[22] D. Ning, S. Sun, H. Du, W. Li, and W. Li, "Control of a multiple-DOF vehicle seat suspension with roll and vertical vibration," *Journal of Sound and Vibration,* vol. 435, pp. 170-191, 2018.

[23] R. Rosli, Z. Mohamed, and G. Priyandoko, "Semi Active Seat Suspension System using Modified Intelligent Active Force Control," *International Journal of Automotive and Mechanical Engineering,* vol. 18, no. 1, pp. 8498–8504-8498–8504, 2021.

[24] X. Zhang, L. Liu, and Y. J. Liu, "Adaptive fuzzy fault‐tolerant control of seat active suspension systems with actuator fault," *IET Control Theory & Applications,* vol. 15, no. 8, pp. 1104-1114, 2021.

[25] K. Wu, C. Ren, and Y. Chen, "Time-delay vibration reduction control of 3-DOF vehicle model with vehicle seat," *Applied Sciences,* vol. 11, no. 20, p. 9426, 2021.

[26] P. Xie, Y. Che, Z. Liu, and G. Wang, "Research on Vibration Reduction Performance of Electromagnetic Active Seat Suspension Based on Sliding Mode Control," *Sensors,* vol. 22, no. 15, p. 5916, 2022.

[27] M. Issa and A. Samn, "Passive vehicle suspension system optimization using Harris Hawk Optimization algorithm," *Mathematics and Computers in Simulation,* vol. 191, pp. 328-345, 2022.

[28] H. Du, W. Li, and N. Zhang, "Integrated seat and suspension control for a quarter car with driver model," *IEEE transactions on vehicular technology,* vol. 61, no. 9, pp. 3893-3908, 2012.